International Journal of Mechanical Sciences 66 (2013) 45–54

Contents lists available at SciVerse ScienceDirect

International Journal of Mechanical Sciences

journal homepage: www.elsevier.com/locate/ijmecsci

Buckling of sandwich columns reinforced by triaxial weave fabric composite skin-sheets

Ahmad B.H. Kueh *

Construction Research Centre, Universiti Teknologi Malaysia, 81310 Skudai, Johor, Malaysia

ARTICLE INFO

Article history:
Received 18 February 2011
Received in revised form
16 October 2012
Accepted 19 October 2012
Available online 1 November 2012

Keywords:
Triaxial weave fabric
Sandwich structure
Volume segmentation
Mechanical property
Buckling

ABSTRACT

This paper investigates computationally the buckling of simply supported sandwich columns constructed using elastic cores reinforced by skin-sheets of triaxial weave fabric (TWF) composites. A novel computationally cheap volume segmentation based thin plate model for the elastic properties of TWF is first developed. The predicted elastic properties of TWF exhibit quasi-isotropic behavior and correlate well with published numerical and measured results. Having demonstrated strong agreement with established results, these properties are then employed in the use of a plate on elastic foundation concept to study the stability of sandwich columns under a uniaxially compressed load environment. The parametric study comprises the effects of thickness, aspect ratio, and modulus of the sandwich core (treated as an elastic foundation), as well as the inclusion of the effects of the initial in-plane and out-of-plane imperfections of the skin-sheets on the critical buckling load. Remarkable dependencies of the critical buckling load on these parameters are demonstrated, due to both independent and wedding actions, noting that a perturbation due to out-of-plane imperfections has been observed to be the most significant contributor to reduction in compressive resistance.

1. Introduction

The increasing trend towards smaller and more highly performing spacecraft for use in geosynchronous communication satellites and space exploration has fueled the need for light and stable materials in the structural applications of these advanced technologies. In the material selection process, textile composites have been the central attraction for fulfilling such a demand because they are superior to unidirectional (UD) composites not only in mass reduction but also in terms of their engineering performances such as out-of-plane stiffness, strength, and toughness, due to their interlocking characteristic. A comparative study of the weight savings achieved through the use of composite solar array panels, relative to aluminum panels, has been conducted by Gronet et al. [1] for honeycomb sandwich construction, from which equal stiffnesses have been exhibited by 8-ply UD and only 1-ply triaxial weave fabric (TWF) composite materials. In general, the panels reinforced by triaxial weave are consistently 5–10% lighter than thin 8-ply UD panels. They are 10–70% lighter than aluminum panels, depending on the thickness of the aluminum skin-sheets.

A sample of cured single-ply TWF composite is presented in Fig. 1, in which tow reinforcements are arranged and woven in three in-plane directions: 0°, $+60^\circ$, and -60°. Due to this architectural configuration, the composite, which is produced by the triaxial weaving method, is structurally superior to most conventional biaxially woven fabric (BWF) materials in terms of one ply comparison where in-plane shear loads are better resisted, a behavior which is attributable to the existence of $\pm 60^\circ$ off-axis tows. Also, about one-half of the volume in TWF is taken by hexagonal voids. These voids provide a reduction in mass per surface area and considerably increase the formability of the material, a property essential for application in structures with multiple geometric constraints.

Unlike BWF, whose mechanical behavior can be satisfactorily estimated using standard laminated theory, the aforementioned structural configurations of TWF, though attractive in performance, have imposed somewhat more subtle characteristics, requiring careful exercise in analytical or numerical formulation for the prediction of its material properties. This has generated research interest and resulted in several studies being carried out in the past few years to examine primarily its tensile behavior. Among these researches is Fujita et al. [2], who reported from experimental and beam network modeling approaches that TWF demonstrates a quasi-isotropic behavior in its initial stiffness. On analytical grounds, three mathematical models were considered by Hoa et al. [3], namely, the crimp model, the upper bound and lower bound variational models, and the laminate model, to determine the tensile elastic constants of TWF, from which fairly

* Tel.: +60 7 5538673; fax: +60 7 5576841.
E-mail addresses: ak_sibu@yahoo.com, kbhahmad@utm.my

0020-7403/$ - see front matter © 2012 Elsevier Ltd. All rights reserved.
http://dx.doi.org/10.1016/j.ijmecsci.2012.10.007

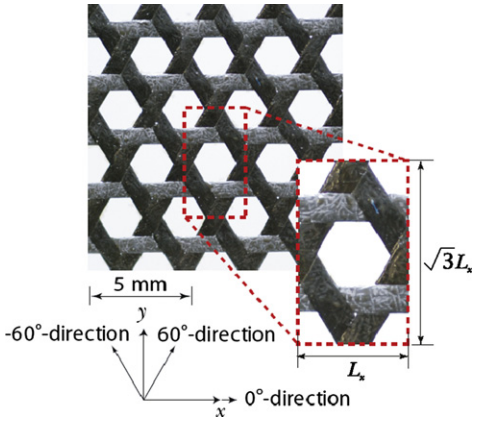

Fig. 1. Small piece of single-ply TWF composite, highlighting the unit cell.

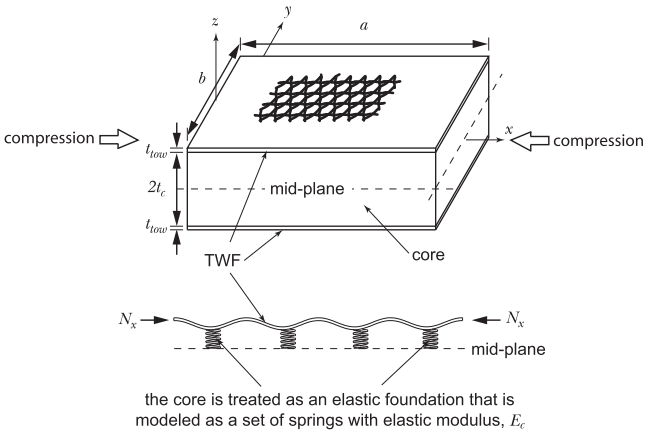

Fig. 2. Sandwich column subjects to compression load. TWF, a wavy and thin skin-sheet, is modeled as laterally restrained by a core that is treated as an elastic foundation with elastic modulus, E_c.

satisfactory agreements were exhibited in comparison to the outcomes of experiments conducted by them. In a similar vein, solid finite elements were developed by Zhao and Hoa [4] and Zhao et al. [5] to explore the size effects on the tensile properties. Finite element numerical analysis was carried out by D'Amato [6] to examine the contribution of tows in different angles to the overall stiffness.

Often, an otherwise good model cannot be widely used due to the complexity in the model set-up and the need for a time-consuming analysis. Most previously developed models, especially those of solid element types, require long formulation and usually extensive computational analysis. Several of these issues have been recently discussed by Kueh [7], in which an analytical fitting free hyperelastic energy density based model for TWF has been developed for convenience of the description of non-linear stress–strain relationship, circumventing and saving on costs due to iterative computation. Such a tradition is continued in this paper, noting the fact that it is of primary importance to devise a simple analytical model that captures satisfactorily both the complex geometry and the mechanical behavior of the material for widespread use, adopting a less laborious model implementation especially during the stage of material properties characterization. In addition, it is worth mentioning that none of the previous researches had studied the stability of this composite when used as the skin-sheets for a sandwich column. Motivated by these considerations, the present paper aims to study the mechanical behavior, in particular, the compressive response, of sandwich structures using TWF composites as skin-sheets. Hence, there are two main considerations in the present study:

1. The development of a simple elastic plate model for the mechanical properties of TWF that captures both its geometrical and material aspects (Section 2).
2. The uniaxially compressed stability of a sandwich structure as shown in Fig. 2 that is reinforced by TWF skin-sheets, and is subjected to various changes in the geometry and the material parameters of its core as well as to initial imperfections coming from the woven nature of the skin material (Section 3).

2. Determination of elastic properties of TWF

2.1. Determination of volume segment of composite tows in a unit cell

The in-plane geometrical parameters of a unit cell of TWF are shown in Fig. 1. A direct way of determining the volume of composite tows in a unit cell, without the contribution of voids, and assuming the tow center lines to be all coplanar, is by denoting the volume occupied by tows by

$$V_{tow} = 6L_x A_{tow} \tag{1}$$

where L_x and A_{tow} are the width of the unit cell and the cross-sectional area of single tow, respectively. The total volume enclosing the unit cell takes the form

$$V_{cell} = \sqrt{3}L_x^2 T \tag{2}$$

where T denotes the total thickness of the unit cell. Note that Eq. (2) includes the contributions from both the solid and the void. The volume segment of tows or solid contained within a unit cell, V_s^f, is then simply the ratio, V_{tow}/V_{cell}.

To characterize V_s^f, it is necessary to be well informed of the material type. In the present study, we investigate TWF of SK-802 fabric type similar to that studied by Kueh [8]. The composite tow is assumed transversely isotropic and is made of T300 carbon fiber and Hexcel 8552 matrix, the material properties of which are listed in Table 1. For single-ply TWF that has a thickness of 0.156 mm and a fiber volume fraction of 0.65 as well as L_x=3.12 mm and A_{tow} = 0.0626 mm^2 [8], V_s^f=0.45.

Table 1
Material properties of T300/Hexcel8552 composite [8].

E_1 (N/mm^2)	E_2 (N/mm^2)	G_{12} (N/mm^2)	G_{23} (N/mm^2)	ν_{12}
153,085	12,873	4408	4384	0.260

2.2. Elastic plate model for single-ply TWF

2.2.1. Elastic model for a wavy, unidirectional composite lamina

Consider a unidirectional fiber reinforced lamina that is subjected to an initial waviness as shown in Fig. 3. Let the initial shape be described by a sinusoidal wave equation

$$w_o = A_p \sin\left(\frac{2\pi x}{L_x}\right) \tag{3}$$

where A_p and L_x are the wave amplitude and the wavelength, respectively. Here, the amplitude of the wave is half that of the tow thickness. Note that the wavelength coincides with the width

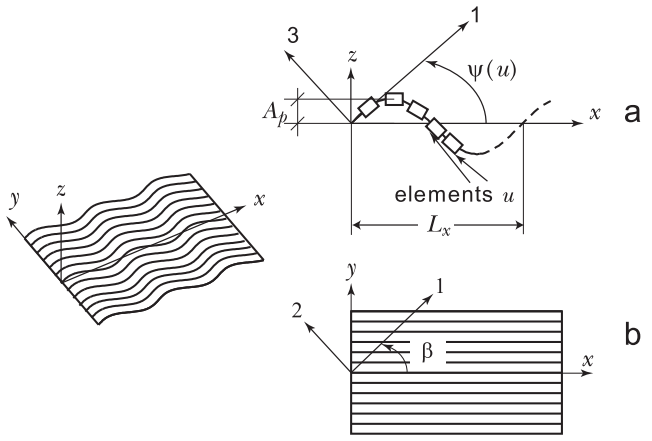

Fig. 3. Transformations of material expressions for a wavy unidirectional fiber reinforced lamina. (a) Transformation about *y*-axis for fiber waviness. (b) Transformation about *z*-axis for off-axis fibers.

of the unit cell. The initial imperfection angle, ψ, is obtained as follows:

$$\psi = \tan^{-1}\left[\frac{2\pi A_p}{L_x}\cos\left(\frac{2\pi x}{L_x}\right)\right] \tag{4}$$

Having presented the geometrical description of the waviness, we shall next treat the associated material expression. The 3D stress–strain relation of a transversely isotropic material is characterized by

$$\begin{Bmatrix}\sigma_{11}\\ \sigma_{22}\\ \sigma_{33}\\ \tau_{23}\\ \tau_{13}\\ \tau_{12}\end{Bmatrix} = \begin{bmatrix} C_{11} & C_{12} & C_{12} & 0 & 0 & 0\\ C_{12} & C_{22} & C_{23} & 0 & 0 & 0\\ C_{12} & C_{23} & C_{22} & 0 & 0 & 0\\ 0 & 0 & 0 & (C_{22}-C_{23})/2 & 0 & 0\\ 0 & 0 & 0 & 0 & C_{55} & 0\\ 0 & 0 & 0 & 0 & 0 & C_{55}\end{bmatrix}\begin{Bmatrix}\varepsilon_{11}\\ \varepsilon_{22}\\ \varepsilon_{33}\\ \gamma_{23}\\ \gamma_{13}\\ \gamma_{12}\end{Bmatrix} \tag{5}$$

or, in short,

$$\{\sigma\} = [C]\{\varepsilon\} \tag{6}$$

where σ_{ij}, C_{ij}, and ε_{ij} are the stress components, the stiffness terms, and the strain components, respectively.

A transformation of the stiffness matrix $[C]$ is necessary, due to the initial waviness, to project the local stiffnesses in accordance with the waveform of the tows so that they can be expressed in terms of the global coordinate configuration. Such a task is performed with the discretization and description of the transformation of a wavy lamina in a piecewise fashion, as shown in Fig. 3a. Denoting the number of discretized elements by u, the transformed stiffness matrix is

$$[\overline{C}] = \frac{1}{u}\sum_{u=1}^{u}[T_\psi]^{-1}[C][T_\psi]^{-T}$$

$$[T_\psi] = \begin{bmatrix} c^2 & 0 & s^2 & 0 & 2cs & 0\\ 0 & 1 & 0 & 0 & 0 & 0\\ s^2 & 0 & c^2 & 0 & -2cs & 0\\ 0 & 0 & 0 & c & 0 & -s\\ -cs & 0 & cs & 0 & c^2-s^2 & 0\\ 0 & 0 & 0 & s & 0 & c\end{bmatrix} \tag{7}$$

Here, $[T_\psi]$ is the transformation matrix about the *y*-axis where

$$c = \frac{1}{(1+\hat{t}^2)^{1/2}}, \quad s = \frac{\hat{t}}{(1+\hat{t}^2)^{1/2}}$$

$$\hat{t} = \tan(\psi) = \frac{2\pi A_p}{L_x}\cos\left(\frac{2\pi x}{L_x}\right) \tag{8}$$

The computed $[\overline{C}]$ is averaged over the chosen number of discretized elements. When the form is that of a thin composite where the out-of-plane stress components can be neglected ($\sigma_{33}=\tau_{23}=\tau_{13}=0$), the inverse of the transformed stress–strain relation can be expressed as

$$\begin{Bmatrix}\varepsilon_{11}\\ \varepsilon_{22}\\ \gamma_{12}\end{Bmatrix} = \begin{bmatrix}\overline{S}_{11} & \overline{S}_{12} & 0\\ \overline{S}_{12} & \overline{S}_{22} & 0\\ 0 & 0 & \overline{S}_{66}\end{bmatrix}\begin{Bmatrix}\sigma_{11}\\ \sigma_{22}\\ \tau_{12}\end{Bmatrix} \tag{9}$$

where

$$\overline{S}_{11} = c^4S_{11}+c^2s^2(2S_{12}+S_{55})+s^4S_{22}, \quad \overline{S}_{12} = c^2S_{12}+s^2S_{23}$$
$$\overline{S}_{22} = S_{22}, \quad \overline{S}_{66} = 2s^2(S_{22}-S_{23})+c^2S_{66} \tag{10}$$

and

$$S_{11} = 1/E_1, \quad S_{12} = -\nu_{21}/E_2 = -\nu_{12}/E_1, \quad S_{22} = 1/E_2$$
$$S_{23} = -\nu_{32}/E_3 = -\nu_{23}/E_2, \quad S_{44} = 1/G_{23} = 2(1+\nu_{23})/E_2$$
$$S_{55} = S_{66} = 1/G_{12} \tag{11}$$

Here, E_i, ν_{ij}, and G_{ij} ($i,j=1,2,3$. Note that subscripts 2 and 3 in the material constants are interchangeable for a transversely isotropic material) are, respectively, Young's moduli, Poisson's ratios, and the shear moduli of the composite lamina. It is essential to note that due to consideration of the out-of-plane waviness, neither G_{23} nor ν_{23} vanishes and therefore it is made one of the independent engineering terms.

The transformed stiffnesses $[\overline{S}]$ given in Eq. (10) are due to the inclination of the composite with respect to the *x*-axis. For TWF, there exists also in-plane off-axis fibers, requiring a second transformation, in this case, about the *z*-axis. For the compliance matrix, such a transformation can be achieved with the following:

$$[\widehat{S}] = [T_\beta]^T[\overline{S}][T_\beta], \quad [T_\beta] = \begin{bmatrix}\widehat{c}^2 & \widehat{s}^2 & 2\widehat{c}\widehat{s}\\ \widehat{s}^2 & \widehat{c}^2 & -2\widehat{c}\widehat{s}\\ -\widehat{c}\widehat{s} & \widehat{c}\widehat{s} & \widehat{c}^2-\widehat{s}^2\end{bmatrix} \tag{12}$$

where $\widehat{c}=\cos(\beta)$ and $\widehat{s}=\sin(\beta)$. β is the transformation angle about the *z*-axis as defined in Fig. 3b. It follows that

$$[\widehat{C}] = [\widehat{S}]^{-1} \tag{13}$$

A convergence investigation is conducted to first determine a sufficient number of discretized elements for the computation of the elastic properties. Fig. 4 shows the relationships of the longitudinal transformed stiffness, $\overline{C}_{11}$, and its computation residual with the number of discretized elements, u. The residual is obtained as the percentage of the difference for each currently computed $\overline{C}_{11}$ value from the previous one. Obviously, there is a reduction in the percentage of the residual as the number of discretized elements increases. It is evident that 200 elements are sufficient for the present model. Nonetheless, 300 elements will

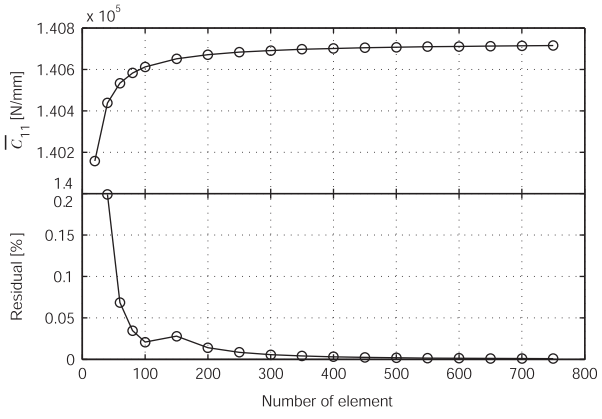

Fig. 4. Convergence of $\overline{C}_{11}$ versus the number of elements.

be used in our computations hereafter. Note that an increase in the number of elements has little effect on the computation time, an advantage over existing numerical models that is worthy of notice.

2.2.2. The constitutive equation of TWF

The constitutive equation of a composite plate that is thin and is multi-directionally reinforced in a layered form is customarily expressed in terms of the ABD matrix:

$$\begin{Bmatrix} N \\ - \\ M \end{Bmatrix} = \left[\begin{array}{c|c} A & B \\ \hline B & D \end{array}\right] \begin{Bmatrix} \varepsilon \\ - \\ \kappa \end{Bmatrix} \tag{14}$$

Here, A,B, and D (3×3 matrix each) represent the in-plane (*stretching and shearing*), coupling, and out-of-plane (*bending and twisting*) stiffnesses of the material, respectively. The ABD matrix relates the mid-plane forces and moments per unit length N_x, N_y, N_{xy} and M_x, M_y, M_{xy} to mid-plane strains $\varepsilon_x,\varepsilon_y,\gamma_{xy}$ and curvatures $\kappa_x,\kappa_y,\kappa_{xy}$. Such a material model will be adopted in the computation of the elastic behavior of TWF.

A calculation of the ABD matrix that treats TWF as a laminate of three layers of material can lead to a significantly overestimated evaluation of its elastic properties. This highly deviant estimation is attributed to the mistreatment of the number of tow, which constitutes the thickness of the TWF, in the calculation. This is explained as follows. The cross-sectional view of the through thickness stacking of tows for TWF can be seen in Fig. 5a. It is obvious that at each interwoven region, there are only two tows in the thickness direction. Since the ABD matrix is a function of thickness, a high deviation in the definition of the thickness can yield a considerable disagreement in the resulting value with the correct properties. Also, the neglect of the hexagonal voids spread across the volume of the TWF, if not captured explicitly in the calculation, can be another factor contributing to an erroneous prediction.

The computation of an alternative ABD matrix for TWF that addresses these issues can be performed on the basis of the volume contribution of each sub-element in all three tow directions. The designations of these sub-elements are highlighted in Fig. 5b. The total volume of the solid in one unit cell, assuming a rectangular cross-section, is given by

$$V_{tot} = 2(V_0+2V_{60}+4V_{rhom})+8V_{tri} = 6b_{tow}L_x t_{tow} \tag{15}$$

where b_{tow} and t_{tow} are the width and thickness of the tow, respectively, V_0 and V_{60} are the volumes of 0°- and 60°-tows (1-tow element), respectively, and V_{rhom} and V_{tri} are the volumes of rhombic and triangular regions, respectively. The volume segments of the sub-elements within one unit cell are as follows:

1. Volume segment of 0°-direction tow (1-tow element),

$$V_0^f = \frac{2V_0}{V_{tot}} = \frac{3L_x-4\sqrt{3}b_{tow}}{9L_x} = V_{60}^f = V_{-60}^f \tag{16}$$

2. Volume segment of 0/60, −60/0, or rhombic elements (2-tow element),

$$V_{rhom}^f = \frac{4V_{rhom}}{V_{tot}} = \frac{4\sqrt{3}b_{tow}}{9L_x} = V_{0/60}^f = V_{-60/0}^f = V_{tri}^f \tag{17}$$

For $b_{tow}=0.803$ mm, the volume segments of 0°-tow, 60°-tow, and −60°-tow, are $V_0^f = V_{60}^f = V_{-60}^f = 0.135$. For the interwoven elements (0/60, −60/0, 60/−60), the volume segments are 0.198. Taking these volume segments into account, A_{ij} and D_{ij} for the ABD matrix can be expressed as

$$\begin{aligned} A_{ij} &= t_{tow}V_s^f(V_1^f+2V_2^f)(\widehat{C}_{ij}^0+\widehat{C}_{ij}^{60}+\widehat{C}_{ij}^{-60}) \\ D_{ij} &= \frac{t_{tow}^3V_s^f}{12}(V_1^f+8V_2^f)(\widehat{C}_{ij}^0+\widehat{C}_{ij}^{60}+\widehat{C}_{ij}^{-60}) \end{aligned} \tag{18}$$

where V_1^f and V_2^f are the volume segments of 1- and 2-tow elements, respectively, $\widehat{C}_{ij}^k$ is the global stiffness as defined in Eq. (13) (k for 0°, 60°, and −60° tows). For a symmetric and balanced stacking sequence, such as that found in TWF, the in-plane and out-of-plane material descriptions are decoupled, i.e., $B_{ij}=0$. The inclusion of the volume segment of the composite tow in a unit cell, V_s^f (Section 2.1), in Eq. (18) takes into account the contribution of the hexagonal voids in the material. Note that $V_2^f=0.198/2$ for the 2-tow elements as each tow is considered separately.

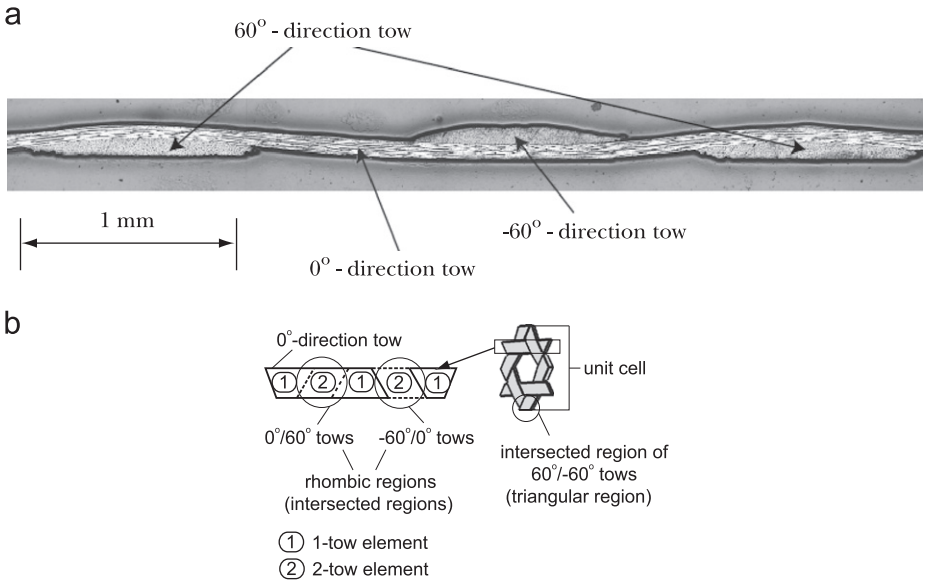

Fig. 5. (a) Micrograph of section along the tow of a cured TWF composite. (b) Region division of unit cell emphasizing the 1-tow element regions, the intersected rhombic regions (2-tow element; 0°/60° and −60°/0° tows), and the triangular regions (2-tow element; 60°/−60° tows).

Table 2
Comparison of the predicted global stiffnesses with the measured results.

Method	S_x (N/mm)	S_{xy} (N/mm)	D_x (N/mm)
Model	1907.43	722.12	2.692
Measured (average) [8]	2111	777	2.077

Considering the above, the constitutive relation of TWF can be evaluated from Eq. (18):

$$\begin{Bmatrix} N_x \\ N_y \\ N_{xy} \\ -- \\ M_x \\ M_y \\ M_{xy} \end{Bmatrix} = \left[\begin{array}{ccc|ccc} 2126.13 & 681.89 & 0 & 0 & 0 & 0 \\ 681.89 & 2126.13 & 0 & 0 & 0 & 0 \\ 0 & 0 & 722.12 & 0 & 0 & 0 \\ \hline 0 & 0 & 0 & 3.001 & 0.962 & 0 \\ 0 & 0 & 0 & 0.962 & 3.001 & 0 \\ 0 & 0 & 0 & 0 & 0 & 1.019 \end{array}\right] \begin{Bmatrix} \varepsilon_x \\ \varepsilon_y \\ \varepsilon_{xy} \\ -- \\ \kappa_x \\ \kappa_y \\ \kappa_{xy} \end{Bmatrix} \tag{19}$$

where the units are N and mm. The computed ABD matrix has a number of characteristics. First, the matrix itself is symmetrical. Second, the sub-matrices $[A]$ and $[D]$ are both symmetric. Also, both the $[A]$ and $[D]$ satisfy the conditions met by a quasi-isotropic plate, namely $A_{11}=A_{22}$; $A_{66}=(A_{11}-A_{12})/2$ and $D_{11}=D_{22}$; $D_{66}=(D_{11}-D_{12})/2$.

The global extensional, shear, and bending stiffnesses of TWF can be, respectively, expressed as

$$S_x=\frac{1}{a_{11}},\quad S_{xy}=\frac{1}{a_{66}},\quad D_x=\frac{1}{d_{11}} \tag{20}$$

using a_{11}, a_{66}, and d_{11}, the inverse values of Eq. (19). The model can be easily programmed and implemented using any available commercial mathematical software, noting that the simplicity of the model can be useful especially when dealing with an analysis of a structure that involves TWF.

Table 2 lists the stiffnesses computed from the present model and the measured values from [8]. A good correlation can be seen from the comparison. Also, based on the geometric and the material properties studied by Hoa et al. [3], the present model predicts a Young's modulus of 37.5 GPa. This is in close agreement with the computed and measured values, which are 37.3 GPa and 39 GPa, noting that the current model differs in terms of its unit cell definition and the details of computation as well as derivation from where the constitutive expression of TWF is expressed with a plate-like composite description, the ABD matrix, which is convenient when finite plate or shell elements are in use. Also, taking into account the solid volume contribution, i.e., discounting the void, the computation is carried out numerically in an algebraic manner rather than analytically, accelerating the computational process and circumventing the possibility of encountering non-integrable functions. Furthermore, a Young's modulus of 39.4 GPa is computed for the material investigated by Zhao et al. [5]. This value agrees well with their maximum measured value, $E_x=37.87$ GPa.

3. Stability of sandwich columns with TWF as skin-sheets

3.1. Force-deformation relationship

For a special orthotropic plate such as TWF where $A_{16}=A_{26}=D_{16}=D_{26}=B_{ij}=0$, the in-plane deformations are uncoupled from the out-of-plane transverse deformation. Hence, we shall solve the governing equation that contains only the derivatives of the transverse deformation. Consider a sandwich structure using TWF composites as wavy skin-sheets bonded to an elastic foundation that is modeled as a set of continuous springs with stiffness E_c, as shown in Fig. 2. The governing equation for such a sandwich structure plus the prescription of a uniformly distributed in-plane unidirectional compression, N_x, is

$$D_{11}\frac{\partial^4 w_1}{\partial x^4}+\overline{D}\frac{\partial^4 w_1}{\partial x^2\partial y^2}+D_{22}\frac{\partial^4 w_1}{\partial y^4}+Kw_1+N_x\frac{\partial^2 w_t}{\partial x^2}=0 \tag{21}$$

where w_1 and w_t are the transverse deformation from the initial wavy shape and the total transverse deformation (w_o+w_1), respectively. w_o is the initial waviness, K is the modulus of the elastic foundation and $\overline{D}=2(D_{12}+2D_{66})$. The modulus K is defined as the force developed by an elastic foundation per unit area and per unit deflection at a point. In the current case, it is described using a set of springs, evenly distributed under the TWF plate, with stiffness resembling that of the one-parameter Winkler foundation [9,10]. We therefore express the foundation modulus as $K=E_c(1/a+1/b+1/t_c)$, a function of the core's Young's modulus, E_c, and its geometric dimensions: a, b, and t_c. They are, respectively, its lengths in the x- and y-direction, and one-half of the thickness. Since TWF occupies the same surface area of the core in the x- and y-direction, a and b are applicable for the skin-sheets as well. Note that, in Eq. (21), the effect of N_x on the bending depends not only on w_1 but also on w_o. The dependencies of D_{ij} and K on w_o are relaxed, as they are only affected by the change in curvature coming from w_1.

Consider now a sandwich column with a rectangular cross-section that is simply supported on all four edges. The boundary conditions can be simply satisfied by letting the extra transverse deformation, w_1, be

$$w_1=A_{mn}\sin\left(\frac{m_1\pi x}{a}\right)\sin\left(\frac{n_1\pi y}{b}\right) \tag{22}$$

where m_1 and n_1 are the numbers of half-waves in the x- and y-direction, respectively. Suppose the initial waviness of TWF takes the following form:

$$w_o=A_p\sin\left(\frac{m_o\pi x}{a}\right)\sin\left(\frac{n_o\pi y}{b}\right) \tag{23}$$

We introduce m_o and n_o as the initial numbers of half-waves in the corresponding directions. The relationship of the uniformly distributed in-plane compression load and the corresponding deflection can be found by substituting Eqs. (22) and (23) into Eq. (21) as well as by performing the corresponding differentiations and rearrangements, to obtain

$$N_x=\frac{D_b\zeta}{\pi^2a^2b^4} \tag{24}$$

where

$$\zeta=w_1/(m_1^2w_o+m_1^2w_1)$$
$$D_b=D_{11}m_1^4\pi b^4+m_1^2\pi^4n_1^2a^2b^2\overline{D}+D_{22}n_1^4\pi^4a^4+Ka^4b^4 \tag{25}$$

In a non-dimensional form, we have

$$\overline{N_x}=\frac{D_K}{\dfrac{m_o^2w_o}{a}+m_1^2\overline{w}}\overline{w} \tag{26}$$

where

$$D_K=m_1^4\pi^4+\frac{2m_1^4\pi^4n_1^2a^2D_b}{b^2D_{11}}+\frac{n_1^4\pi^4a^4D_{22}}{b^4D_{11}}+\frac{Ka^4}{D_{11}} \tag{27}$$

Here, $\overline{N_x}=N_x\pi^2a^2/D_{11}$, $D_b=\overline{D}/2$, and $\overline{w}=w_1/a$.

3.2. Comparison with experiment

Having just obtained Eq. (26), we proceed to compare the present model with the measured value from the experimental study conducted by Kueh [8]. In the experiment, nearly square

TWF sheets, of size 40 mm wide by 55 mm long, bonded to a 20 mm thick polyvinyl chloride (PVC) foam core, were used for the purpose of minimization of edge effects. The extensional and the shear moduli of the core were given as E_c=295 MPa and G_c=110 MPa, respectively.

Here, we shall look at the critical buckling load that comes from Eq. (26) by adopting the notion that the critical value of compression when a plate becomes unstable can be obtained when the applied load develops in an asymptotic manner at which the deflection tends to grow indefinitely [11]. It has been discovered from detailed investigation that this load changes in accordance with m_1. In the present model, we use an m_1 value by employing the assumption that there is no occurrence of interfacial detachment between TWF and core, and that the failure is by microbuckling, not global. It is of importance to grasp that the obtained solutions, by invoking the vanishing of the derivative of the load deformation relation, are of a complex nature whose conjugate products are negative. Adopting the notion that there exists only a single minimum buckling load, m_1 must be identically satisfied in a conjugate sense. However, it has been observed from the current model that N_{cr}, i.e., the minimized load intensity, is exerted only when $m_1=m_o$ since a lower m_1 always give a higher N_x, which is considerably greater than that found from measurement. Therefore, in the remainder, the focus will be on TWF plates that are readily formed in accordance with the imperfection waveform, i.e., m_1 follows the initial local imperfection m_o, assuming $n_1=n_o=1$, in the transverse direction. This is a reasonable description since the locally existing imperfection is eventually amplified when subjected to a uniaxial compression. As a result, the column buckles following the initial imperfection state although it may be of concern and shall not escape our view that a different competing mode may overrule this, due to various parametric effects. Such an examination will be the subject of future consideration. It should be noted that, for validation purpose, only the critical value is of interest. The effective buckling load for TWF is obtained by multiplying the acquired critical value by one-third, considering only one-third of the width of the skin-sheet is filled with tows in the direction of the load. Therefore, the corresponding N_{cr} for the skin-sheet is 7.33 N/mm. In comparison, this value is in very satisfactory agreement with the average of the measured buckling load 7.64 N/mm given in [8].

In the case of simple analytical formulae, the fiber microbuckling load calculation [12] predicts correctly the failure mode based on the chosen sandwich column geometry and material studied in [8]. However, the critical load is exaggerated by three times that of the measured value ($N_{cr}=1/3tV_f\sigma_{cr}=$ 24.84 N/mm). Note that one-third has been included in the calculation. The prediction based on the combined buckling mode [12], attributed to the Euler buckling load (P_E) and the core shear buckling load (P_s), is far less favorable. The resulting value, which can be computed by the following:

$$\frac{1}{N_{cr}}=2b\left(\frac{1}{P_E}+\frac{1}{P_s}\right) \tag{28}$$

where

$$P_E=2bS_x\left(\frac{\pi t_c}{a}\right)^2=47.8KN \tag{29}$$

$$P_s\approx 2bt_cG_c=88KN \tag{30}$$

is 387 N/mm. The most likely reason for the overestimation is that these equations only consider the smearing property of the skin-sheet, by treating it as a solid plate, but ignore the existence of voids spreading over the volume of the material.

3.3. Effect of initial waviness

Often, the fabrication of a presumably flat plate is very difficult. A certain degree of imperfection is inevitable, and curvature may be introduced in the material during such a process. The superposition of this imperfection on an existing waviness of the tow can affect the elastic behavior. We define the normalized waviness number, ξ, as the ratio of the imperfect wave amplitude to that of the initial. Ignoring first the parametric variation of the core, an increment in the waviness promotes the reduction of all stiffnesses of TWF: S_x, S_{xy}, and D_x. As a consequence, it leads to a decreased capability of compressive load resistance. Such a phenomenon can be best described with the assistance of Fig. 6a, which shows the relationships between the normalized compressive load and the normalized maximum deflection. The length of the column, a, is set to 56.16 mm, about the same as that used in [8]. The initial slope of the curve reduces gradually, corresponding to the increment of wave amplitude ranging from 0.1% a to 0.5% a. Eventually, all curves go horizontal during which a critical compressive load is achieved. In general, an increase in the waviness number correlates inversely with the compressive load resistance, implying that the waveform of TWF, which has a direct effect on the stiffnesses, plays a substantial role in the buckling load capability.

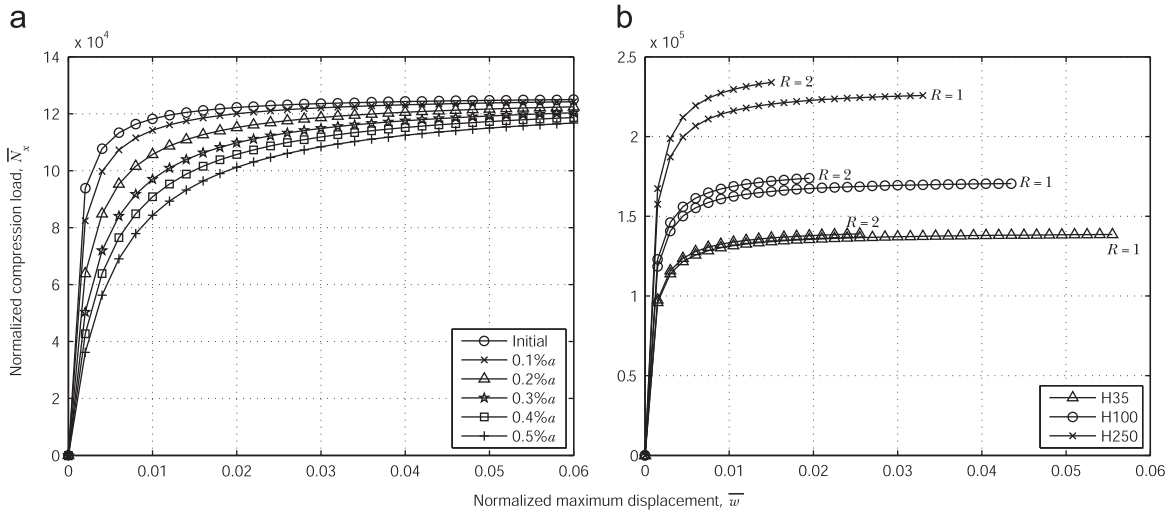

Fig. 6. Normalized compressive load versus normalized maximum displacement curves. (a) Effects of waviness. (b) Effects of core types and aspect ratios.

3.4. Effect of elastic foundation

Let us consider now the influence of parametric changes in the elastic core on the compressive response of the sandwich column. The initial amplitude of TWF is fixed to one-half that of the tow thickness, i.e., no variation in waviness number, ξ. The aim here is to investigate only the effects coming from the variation in the properties of the core. The particular core used for this study is of closed-cell polyvinyl chloride (PVC) foam (tradename: Divinycell). The material properties of the core used in the current study are listed in Table 3.

Introducing the aspect ratio, $R=a/b$, Fig. 6b shows the relationships of the normalized compressive load with the normalized maximum deflection corresponding to different core moduli and aspect ratios for a thickness of $t_c=20$ mm. An enhancement in the modulus of the core has a clear boosting effect on the compressive carrying capacity. The plots for materials with a lower core modulus bifurcate earlier than those with a higher modulus. Observe also, for the same core type, a slightly greater critical buckling load is found for the column with a greater aspect ratio. The difference becomes less pronounced for those using H35. It is worth noting that the termination of each curve is due to the maximum axial strain sustainable by the weave. From all studied cases, the cores with the aspect ratio $R=2$ have a lower maximum normalized transverse deformation, $\overline{w}$, in comparison to those with $R=1$.

If the variation in the core thickness is taken into account, its relationship with the critical buckling load N_{cr} at which the transverse deformation grows indefinitely can be observed in Fig. 7a. Observe again that, for the same core type, a noticeable difference in the critical buckling load is present in high-stiffness cores for two different aspect ratios, $R=1$ and $R=2$. This difference vanishes as the core becomes more compliant. In all cases, the declination in the buckling load N_{cr} directly corresponds to the growth in the core thickness. Columns with a thin and high-stiffness core, H250, exhibit more pronounced responses, that is, a buckling capacity reduction of about 30%, from $t_c=5$ mm to $t_c=10$ mm. This effect is less prominent for the low-stiffness core, especially for H35, where a reduction of 7% is found. The contribution of the core to the improvement of the buckling load is considerably lessened following a drop in the modulus. The buckling loads for all columns are practically unaffected by the core thickness after $t_c=60$ mm.

Fig. 7b presents the curves for the critical buckling load N_{cr} as a function of the sandwich core modulus for different aspect ratios, R, and thicknesses, t_c. All critical buckling loads increase in a linear manner following an increase in the core modulus. The figure shows that the highest range of critical buckling loads comes from those with a high aspect ratio and a thin core. Examining Eq. (27), we observe that increasing the length of the core while reducing both the width and thickness boosts the effective foundation modulus term D_K and hence the compressive capacity. Again, the response coming from the change in aspect ratio is more apparent for columns using the high-modulus core.

Table 3
Material properties of core [13].

Core type	E_c (N/mm^2)	G_c (N/mm^2)
H35	40	12
H100	135	35
H250	300	104

3.5. Effect of in-plane imperfection

Next, a misalignments ranging from 1° to 5° will be considered in the in-plane orientations for 0°-tows and 60°-tows. It is found within this range that (not shown here) the in-plane shear modulus S_{xy} suffers the most reduction, about 10%. This is mainly contributed by the in-plane imperfection in the 60°-tows from the comparison between the weave with no in-plane misalignment and that with 5°. An imperfection in 0°-tows has little effect on S_x and D_x, about a 3% reduction each for 5° misalignment. This observation verifies that adding tows in an off-axis direction, as used in TWF, provides a better shearing resistance than for BWF. Overall, there are slight perturbations in all elastic properties but the effects on the critical buckling load are negligible in comparison to the out-of-plane imperfection reported in Section 3.3. Eq. (21) shows that the buckling load is dominated by the bending stiffnesses, primarily that defined by D_x. Although D_{11}, D_{12}, and D_{66} change with respect to small in-plane imperfections, the bending modulus of the weave D_x has not been much affected. As a result, there does not exist much change in the buckling capability. Therefore, the effects of varying the in-plane misalignment will not be further pursued.

3.6. Effects of combined changes in foundation parameters and wave amplitudes

An investigation of the effects of combined parametric perturbations in the core and the tow waviness will now be reported. Independently, the former increases the critical buckling load and

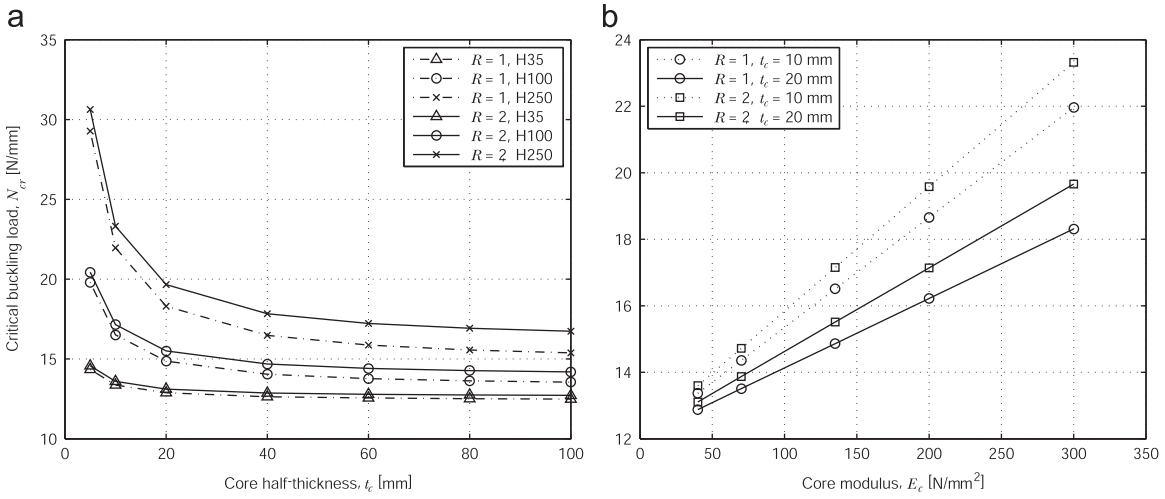

Fig. 7. Effects of changes in elastic foundation parameters. (a) Buckling load versus thickness t_c for different core types and aspect ratios. (b) Buckling load versus core modulus for different aspect ratios and core half-thicknesses.

vice versa for the latter. The effects that come from the alterations of these parameters on TWF are worth investigating as the outcome may not be directly intuitive. We shall be interested in the critical buckling load for an aspect ratio of $R=1$, and thicknesses $t_c=10$ mm and $t_c=20$ mm. Fig. 8 shows that the advancement in the buckling load coming from the core modulus is offset by an increment in the waviness number. Note that the compressive responses for $R=2$ are much the same and hence are not shown here. Next, we shall for convenience focus only on the sandwich column with thickness $t_c=10$ mm. Fig. 9a and b show the relationships of nominal buckling load $\overline{N_{cr}}$ with the waviness number and nominal core modulus, respectively. The nominal buckling load $\overline{N_{cr}}$ is the ratio of the considered N_{cr} to that of its initial, unperturbed state. The nominal core modulus is the value of the considered E_c normalized by the E_c of H35. Fig. 9a shows that the rate of reduction in $\overline{N_{cr}}$ is the highest for the highly compliant core H35. The feature to note here is the slope at which the curve drops, e.g., the H35 curve drops the fastest of all three curves. The more compliant a core, the less lateral support is provided for the skin-sheet, and therefore a lesser buckling load. The plots diverge as the normalized amplitude increases. When the $\overline{N_{cr}}$ are plotted against E_c for a range of waviness numbers, a fairly linear ascending pattern is seen (Fig. 9b). Observe that the curve with the highest imperfection, 0.5% a, exhibits the highest gradient. Therefore, as the imperfection grows, the change in buckling load becomes larger. In general, the stability of the column is prone to be affected by the waviness number in the case of a small imperfection. Conversely, the change in $\overline{N_{cr}}$ is most likely governed by the modulus of the core when highly stiff cores are used as column material.

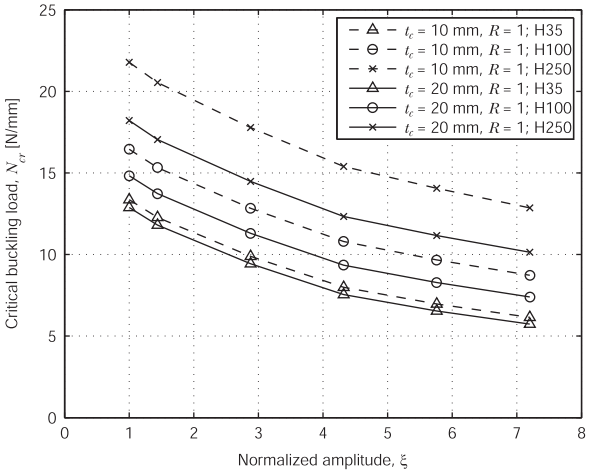

Fig. 8. Critical buckling load as a function of normalized amplitude, ξ, for different core types and core half-thicknesses for $R=1$.

3.7. Parametric perturbations in the specimen studied in [8]

Exceptional dependencies of the buckling load on changes in the geometry and the material characteristics of sandwich column have inspired a further look at the effects of these perturbations in the specimen investigated by Kueh [8].

Here, the modulus of the core, i.e., the elastic foundation stiffness, for the present model has been made equal to that used in the measurement. For the current purpose, we shall only permit small deviations in the properties, which may come from unforeseen uncertainties during the preparation of the specimens. The perturbed parameters are the length, the width, the core half-thickness, and the initial wave amplitude, noting that an alteration in the initial wave amplitude will also affect the bending stiffnesses. The lengths are chosen so that they coincide with the numbers of half-waves, m_o and m_1. The effective buckling loads computed regarding the aforementioned changes are plotted in Fig. 10.

Combined changes in the geometrical parameters of the sandwich column clearly affect the buckling loads. The critical value varies gradually in a downward fashion from the left to the right of the plots. In general, a decrease in the buckling load is characterized by a concerted action of increases in a, b, t_c, and A_p, where the most significant reduction is contributed by the wave amplitude.

4. Conclusion

The stability of a wavy triaxial weave fabric composite that is bonded to an elastic core has been investigated. The elastic constants are first described in terms of a thin plate constitutive equation, the ABD matrix, involving the volume contribution of each segmented element of tow according to its orientation. The computed elastic properties correlate well with the measured

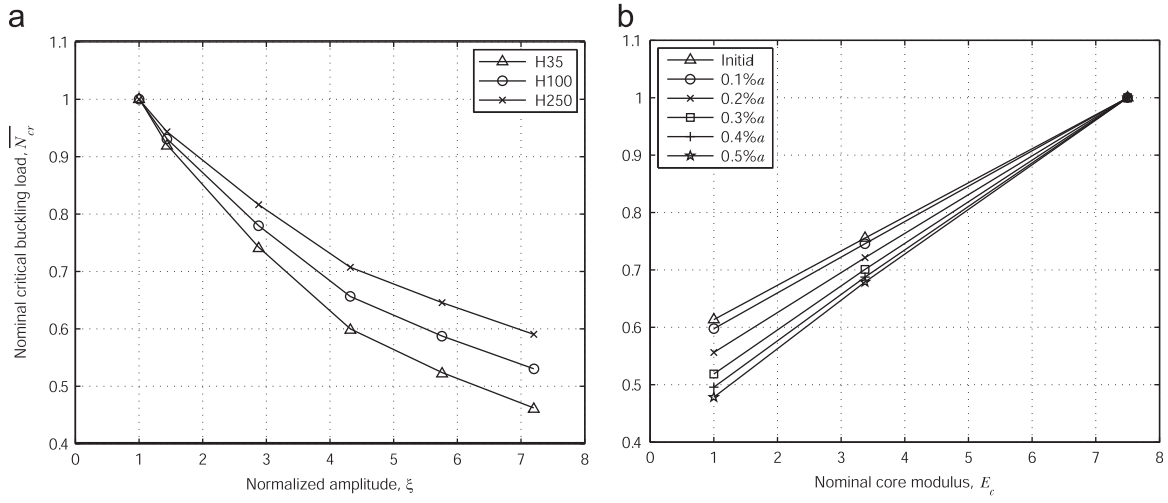

Fig. 9. Correlations of nominal buckling load. (a) With respect to normalized waviness number for different core types. (b) With respect to nominal core modulus for a range of waviness numbers.

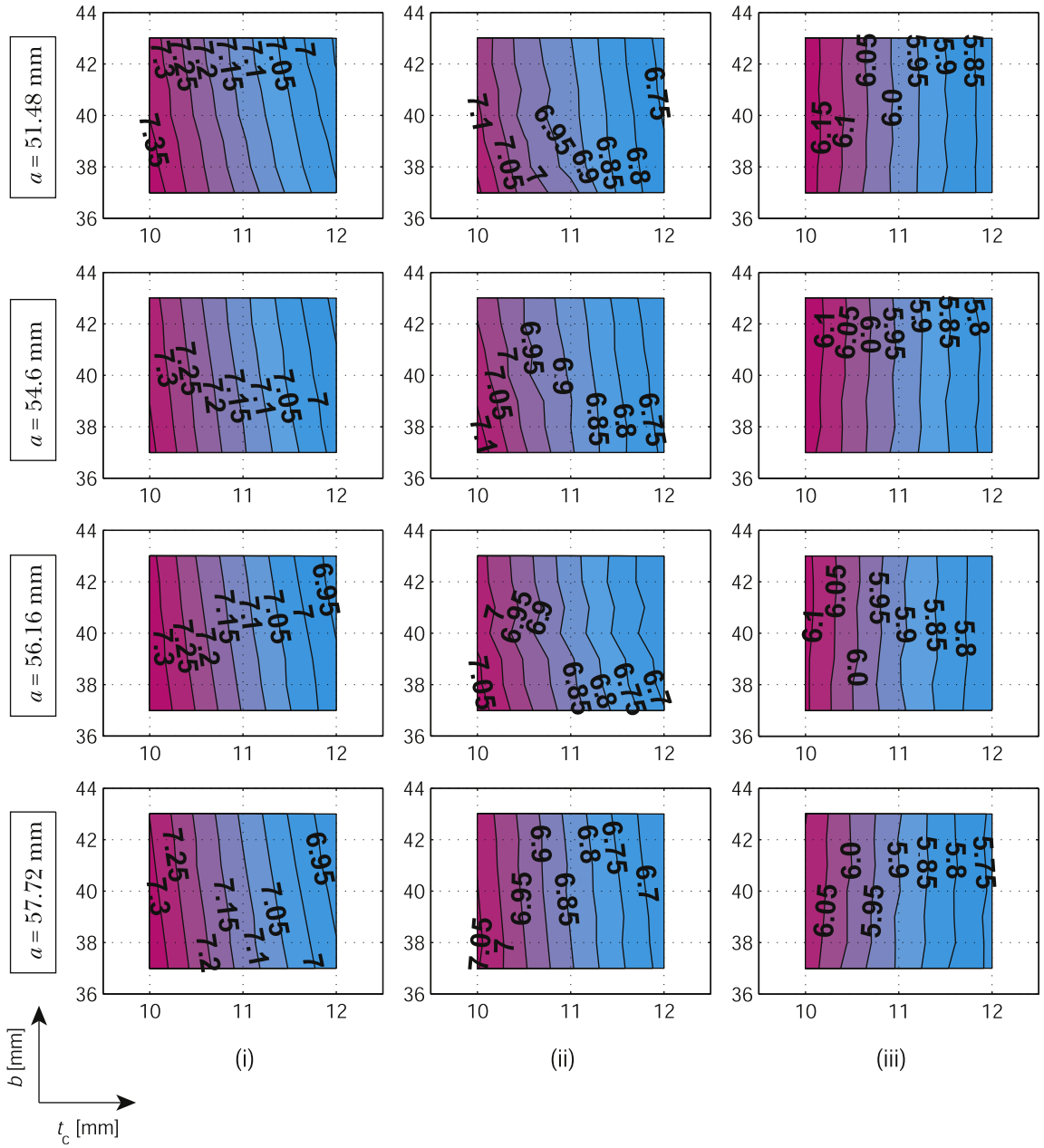

Fig. 10. Effective buckling load contour plots of TWF skin-sheet for different lengths (a=51.48 mm, 54.6 mm, 56.16 mm, and 57.72 mm.) and wave amplitudes ((i) initial amplitude; (ii) 0.1%a; (iii) 0.2%a.) in terms of various widths and core half-thicknesses.

values as well as the numerical results available from the literature. A parametric study of the stability of a simply supported sandwich column was then carried out with regard to the effects on the critical buckling load of the thickness, aspect ratio, and modulus of the sandwich core, as well as the initial in-plane and out-of-plane imperfections of TWF. Independently, an increase in the initial waviness of the weave alone reduces the stiffnesses, leading to a reduction in the compressive load resistance. Without considering the waviness effects, the sandwich core improves the critical buckling load of TWF as a result of the provision of a continuous lateral support. Small misalignments in the in-plane orientations inflict little effect on the buckling load. Combining parametric changes of the core with weave imperfections cause an enhancement of the buckling load, contributed by the core modulus, which is offset by the effects of any increase in the waviness number. For a column with little imperfection, N_{cr} is sensitive to the waviness number. The change in N_{cr} is dominated by the modulus of the core for columns using high-stiffness cores.

Acknowledgment

The author thanks the Ministry of Higher Education (MOHE), Malaysia and Universiti Teknologi Malaysia for Research Grants (FRGS 78435 and RUGS Q.J130000.7122.00J13). Gratitude is extended to Siti Nursarjana Malim for proofreading the manuscript.

References

[1] Gronet MJ, Jensen GA, Hoskins JW. Structures and materials technology needs for communications and remote sensing spacecraft. NASA Contractor Report 198166; 1995.
[2] Fujita A, Hamada H, Maekawa Z. Tensile properties of carbon fiber triaxial woven fabric composites. J Compos Mater 1993;27:1428–42.

[3] Hoa SV, Sheng SZ, Ouellette P. Determination of elastic properties of triax composite materials. Compos Sci Technol 2003;63:437–43.
[4] Zhao Q, Hoa SV. Triaxial woven fabric (TWF) composites with open holes (Part I): finite element models for analysis. J Compos Mater 2003;37:763–89.
[5] Zhao Q, Hoa SV, Ouellette P. Triaxial woven fabric (TWF) composites with open holes (Part II): verification of the finite element models. J Compos Mater 2003;37:849–73.
[6] D'Amato E. Finite element modeling of textile composites. Compos Struct 2001;54:467–75.
[7] Kueh ABH. Fitting-free hyperelastic strain energy formulation for triaxial weave fabric composites. Mech Mater 2012;47:11–23.
[8] Kueh ABH. Thermo-mechanical properties of triaxial weave fabric composites. PhD thesis, Department of Engineering, University of Cambridge; 2007.
[9] Kim SM, McCullough BF. Dynamic response of plate on viscous Winkler foundation to moving loads of varying amplitude. Eng Struct 2003;25:1179–88.
[10] Abdalla JA, Ibrahim AM. Development of a discrete Reissner–Mindlin element on Winkler foundation. Finite Elem Anal Des 2006;42:740–8.
[11] Timoshenko SP, Gere JM. Theory of elastic stability. 2nd ed.McGraw-Hill; 1963.
[12] Fleck NA, Sridhar I. End compression of sandwich columns. Composites Part A: Appl Sci Manuf 2002;33:353–9.
[13] DIAB, Divinycell H technical data sheet.